Scenario-Based Model Predictive Operation Control of Islanded Microgrids

Christian A. Hans, Pantelis Sopasakis, Alberto Bemporad, Jörg Raisch and Carsten Reincke-Collon

***Abstract*— We propose a model predictive control (MPC) approach for the operation of islanded microgrids that takes into account the stochasticity of wind and load forecasts. In comparison to worst case approaches, the probability distribution of the prediction is used to optimize the operation of the microgrid, leading to less conservative solutions. Suitable models for time series forecast are derived and employed to create scenarios. These scenarios and the system measurements are used as inputs for a stochastic MPC, wherein a mixed-integer problem is solved to derive the optimal controls. In the provided case study, the stochastic MPC yields an increase of wind power generation and decrease of conventional generation.**

I. Introduction

Worldwide, decentralized renewable energy production is growing [1]. The power infeed of many of these distributed sources fluctuates, depending on weather conditions. One way to cope with the changed, distributed power generation and the increasing fluctuations over a large network is to partition the grid into small electrical networks, called microgrids (MGs) [2]. To increase the reliability of supply, MGs can be operated in an electrically isolated (islanded) mode, for example, if problems within the transmission network occur [3]. Electrical networks that are always operated in isolated mode due to geographical reasons, e.g., on islands or in rural areas also fit into the class of islanded MGs. In this operation mode, generation, storage and consumption must be balanced locally. Especially in MGs with increased share of intermittent renewable energy sources (RES), providing optimal power setpoints for the units while considering local power balance as well as power and energy constraints is challenging due to high uncertainty of RES infeed.

A natural approach to cope with the uncertainty is to employ forecasts. For load, many solutions based on time-series analysis exist. An overview of five short-term load forecast techniques is given in [4]. Further, in [5] an expert system that connects weather and load for a 24 h ahead forecast is proposed. For the short-term prediction of wind time-series also various models were presented, e.g., in [6].

C. A. Hans is with Technische Universität Berlin, Germany, hans@control.tu-berlin.de

P. Sopasakis and A. Bemporad are with IMT Institute for Advanced Studies Lucca, Italy, {pantelis.sopasakis, alberto.bemporad}@imtlucca.it

J. Raisch is with Technische Universität Berlin and Max-Planck-Institut für Dynamik komplexer technischer Systeme, Germany, raisch@control.tu-berlin.de

C. Reincke-Collon is with Younicos AG, Germany, reincke-collon@younicos.com

Support by the Reiner Lemoine Foundation and the U.S. Department of Energy as part of the Atmospheric Radiation Measurement (ARM) Climate Research Facility is highly acknowledged.

For the operation control of MGs various MPC approaches that employ forecasts have been proposed. The main reason for MPC is the flexibility to incorporate forecasts, and the state of charge of storage devices, as well as the availability of all units. In [7] a two stage stochastic optimization approach for the operation of grid-connected MGs was proposed. A scenario-based approach for grid-connected MGs can be found in [8]. For islanded MGs, in [9] a scheme that uses a robust forecast interval for load, and RES and allows limiting RES infeed was proposed. To decrease conservativeness, [10] extended the approach by considering the dependence of the controls on the predicted states.

The approaches pursued by [7], [8] both suffer of the fact that they are only applicable to grid-connected MGs where the transmission network acts as a slack node. Further, they do not allow to capture the fact that RES could be limited. In contrast, [9], [10] propose schemes for islanded MGs that use the forecast intervals of load and RES and allow a limitation of RES infeed. Even though in [10] the run time costs could be decreased, the approach still leads to conservative results as the forecast probability distribution is not considered.

Combining ideas from time-series based forecasting [11], scenario reduction [12], stochastic optimization [13], and the MG model from [9], our contribution is a scenario-based stochastic MPC for islanded MGs. Taking into account the stochasticity of RES and load forecasts, we provide a solution that reduces the conservativeness of [10].

The remainder of the paper is structured as follows. Moving along the blocks in Fig. 1, in Section II we introduce models used for wind and load forecasts. In Section III, scenario reduction is discussed and in Section IV a scenario-based stochastic MPC approach is described. The numerical case study in Section V then compares the new scheme with the approach from [10] and a reference with perfect forecast.

A. Notation

We define the set $\mathbb{R}_{0+} = \{x \in \mathbb{R} | x \geq 0\}$. The set of natural numbers $\mathbb{N}$ in the closed interval $[k_1, k_2]$ is denoted by $\mathbb{N}_{[k_1,k_2]}$ and the set of Boolean variables by $\mathbb{B} = \{0, 1\}$. Let $\mathrm{diag}(a_1, \ldots, a_n)$ be the diagonal matrix of size $n \times n$ and diagonal entries a_i, $i = 1, \ldots, n$. Further, $\mathbf{0}_{nm}$ is the $n \times m$ matrix of all zeros, $\mathbf{1}_{nm}$ the $n \times m$ matrix of all ones and $\mathbf{I}_n$ the $n \times n$ identity matrix. Accordingly, the $n \times 1$ zero vector is $\mathbf{0}_{n1}$ and the $n \times 1$ vector of ones $\mathbf{1}_{n1}$.

Backshift notation: For a given time-series of data $w_1, w_2, \ldots$ the backshift operator B with $(Bw)_k = w_{k-1}$ for $k \in \mathbb{N}_{[2,\infty]}$ is used to refer to past values. For $j \geq 2$, $B^j = BB^{j-1}$ and hence $(B^j w)_k = w_{k-j}$.

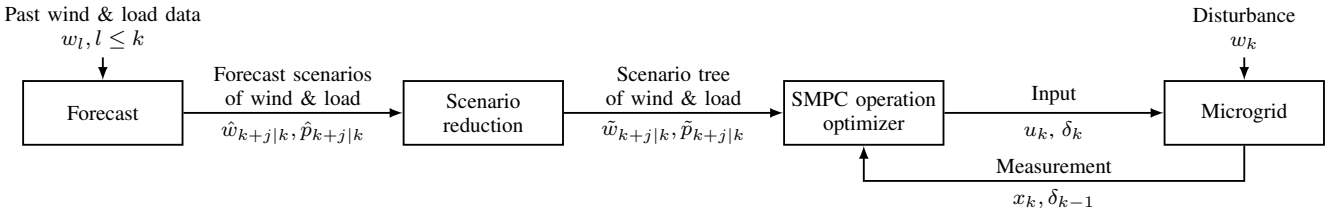

Fig. 1. Forecast with scenario reduction, scenario-based stochastic MPC (SMPC) and MG.

II. Forecast

SARIMA model: As indicated by [11], seasonal autoregressive integrated moving average $\mathrm{SARIMA}(p,d,q,s,P,Q)$ models, with $p,d,q,s,P,Q \in \mathbb{N} \cup \{0\}$ have the form

$$(\phi(B)\Phi(B)(1-B)^d(1-B^s)w)_k = c+(\theta(B)\Theta(B)e)_k, \quad (1)$$

where $e_k = w_k - \hat{w}_k$ is the model error between w_k from the training set and the forecast value $\hat{w}_k$. The polynomial $\phi(B) = (1-\phi_1 B^1 - \ldots - \phi_p B^p)$, $\phi_1, \ldots, \phi_p \in \mathbb{R}$ represents the autoregressive and $\Phi(B) = (1-\Phi_1 B^1 - \ldots - \Phi_P B^P)$, $\Phi_1, \ldots, \Phi_P \in \mathbb{R}$ the seasonal autoregressive part. In (1), $(1-B)^d$ stands for an integrator, $(1-B^s)$ for seasonality and c for trend. Further, $\theta(B) = (1+\theta_1 B^1 + \ldots + \theta_q B^q)$, $\theta_1, \ldots, \theta_q \in \mathbb{R}$, is the moving average part and $\Theta(B) = (1+\Theta_1 B^1 + \ldots + \Theta_Q B^Q)$, $\Theta_1, \ldots, \Theta_Q \in \mathbb{R}$ the seasonal moving average part of the model.

To reduce the complexity and derive a model whose parameters have high statistical significance (indicated by the t-statistic), it can be useful to exclude several lags by setting some coefficients of $\phi(B)$, $\Phi(B)$, $\theta(B)$ and $\Theta(B)$ to zero if they have minor influence and then re-train the model [11]. The model is then referred to as $\mathrm{SARIMA}(\chi_p, d, \chi_q, s, \chi_P, \chi_Q)$, where $\chi_p \subseteq \mathbb{N}_{[1,p]}$ is the set of indices of coefficients ϕ_i, that are not forced to zero and $p \in \chi_p$. The same holds for $\chi_q \subseteq \mathbb{N}_{[1,q]}$ with $q \in \chi_q$, $\chi_P \subseteq \mathbb{N}_{[1,P]}$ with $P \in \chi_P$ and $\chi_Q \subseteq \mathbb{N}_{[1,Q]}$ with $Q \in \chi_Q$. SARIMA models without seasonality and $P = Q = 0$ will be denoted by $\mathrm{ARIMA}(\chi_p, d, \chi_q)$.

A. Wind forecast

Motivated by [6] and [11], for wind speed forecasting a ARIMA model was chosen. The parameters were selected, using the Akaike information criterion (AIC) [11] to evaluate the quality of different models, trained with a dataset of 5000 samples of 30 min mean values from the Azores Island Graciosa, provided by [14]. For the given data, the minimum AIC was found for an $\mathrm{ARIMA}(\chi_p, 0, \chi_q)$ model with $\chi_p = \{1, 3, \ldots, 7, 9\}$ and $\chi_q = \{1, \ldots, 4\}$. The Ljung-Box test [11] for uncorrelatedness of residuals e_k passed with p-value 0.65 . Hence, the proposed model is of adequate complexity. The normality assumption of the residuals of the model could not be confirmed by the Kolmogorov–Smirnov test [11], which failed at the 5 % significance level. Therefore, subsequently Monte Carlo (MC) simulations are used to estimate the forecast probability distribution.

For each MC simulation, random residuals from the training dataset are drawn and added to the forecast. This way, for a high number of simulations, the forecast distribution comes close to the residuals observed in the training. Hence, the forecast probabilities can be expressed without the need to assume normality of the errors. This leads to a purely data-driven setting where no assumptions on the probability density function of the uncertainty need to be imposed.

Forecast evaluation: To test the forecast performance, the trained $\mathrm{ARIMA}(\chi_p, 0, \chi_q)$ model was used to perform 1000 predictions over a horizon $J = 24$, i.e., 12 h. From the wind speed forecast $\hat{v}_{k+j|k}$, $j = 0, \ldots, J$, the wind power $\hat{w}_{k+j|k}$ predicted at time k for $k+j$ was calculated with

$$\hat{w}_{k+j|k}(\hat{v}_{k+j|k}) = \begin{cases} \frac{\hat{v}^3_{k+j|k}}{12^3} & \text{if } \hat{v}_{k+j|k} \in [2.5\,\mathrm{m/s}, 12\,\mathrm{m/s}), \\ 1 & \text{if } \hat{v}_{k+j|k} \in [12\,\mathrm{m/s}, 25\,\mathrm{m/s}), \\ 0 & \text{else,} \end{cases}$$

motivated by [15]. The saturation for values less than 2.5 m/s is an economical optimization by the wind turbine manufacturers. Further, if the nominal power is reached at 12 m/s the maximum infeed, i.e., 1 pu is reached. If the wind-speed is above 25 m/s, wind turbines are turned off for security reasons.

The results of the forecast $\hat{w}_{k+j|k}$ (see Fig. 2 left) were then compared with the test set values w_{k+j}. To assess the forecast quality, the prediction root mean squared error

$$\mathrm{PRMSE}_J(k) = \sqrt{\tfrac{1}{J}\textstyle\sum_{j=1}^{J}(w_{k+j} - \hat{w}_{k+j|k})^2}$$

was calculated for 10^3 predictions with horizon $J = 24$ and the probability distribution of all PRMSE_J was used. The error distribution of all forecasts performed with the $\mathrm{ARIMA}(\chi_d, 0, \chi_q)$ model is shown in Fig. 3. As reference a $\mathrm{ARIMA}(2,0,0)$ model, as proposed by [6], as well as a naïve forecast with $\hat{w}_{k+j|k} = w_k$ were chosen. With mean $\mathrm{PRMSE}_{24} = 0.035\,\mathrm{pu}$, (standard deviation: 0.040 pu), the mean PRMSE_{24} of the $\mathrm{ARIMA}(\chi_d, 0, \chi_q)$ model is about 13 % smaller and the standard deviation about 22 % less than with the naïve method. The $\mathrm{ARIMA}(2,0,0)$ with mean $\mathrm{PRMSE}_{24} = 0.037\,\mathrm{pu}$, (standard deviation: 0.040 pu) lies between the other two approaches. Still, the higher forecast quality of the $\mathrm{ARIMA}(\chi_d, 0, \chi_q)$ approach justifies the additional computational effort.

B. Load forecast

Because of the highly seasonal nature of electric load a SARIMA model was chosen. The parameters of the model were selected using the AIC with training data set of one year of 30 min instantaneous load power values. A minimum AIC was found for a $\mathrm{SARIMA}(\chi_p, d, \chi_q, s, \chi_P, \chi_Q)$ model with $\chi_p = \{1, \ldots, 15\}$, $d = 1$, $\chi_q = \{1, \ldots, 15\}$, $s = 7 \cdot 48$, $\chi_P = \{48\}$, $\chi_Q = \{48, 7 \cdot 48\}$. The coefficients of the model were identified at a high statistical significance, quantified by the t-statistic. The Ljung-Box test passed with

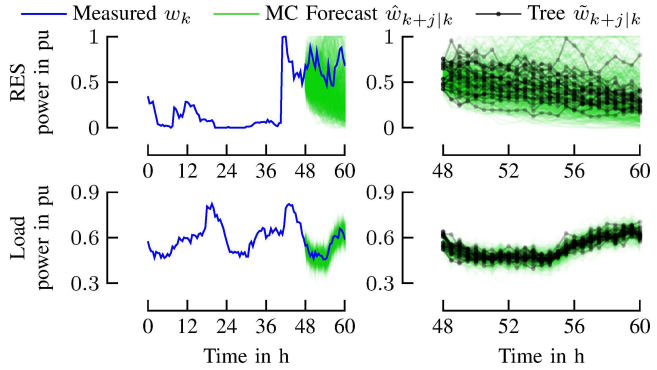

Fig. 2. Wind forecast with $\mathrm{ARIMA}(\chi_p, 0, \chi_q)$ and load prediction with $\mathrm{SARIMA}(\chi_p, d, \chi_q, s, \chi_P, \chi_Q)$ model over a horizon of 12 h. The scenario fan was generated using MC simulations with 500 seeds. The scenario tree was determined using a branching factor $b = (8, 2, 2, 1, \ldots, 1)$.

p-value 0.82 indicating an adequate complexity of the model. Further, the normality of the residuals could not be confirmed by the Kolmogorov–Smirnov test which failed at the 5 % significance level. Therefore, MC simulations with residuals from the load model fit were used to produce the forecast probability distribution.

Forecast evaluation: As test set, 73 days of 30 min instantaneous values were used to assess the quality of 3504 forecasts with horizon $J = 24$. One SARIMA forecast is shown in Fig. 2. Simple seasonal naïve forecast $\hat{w}_{k+j|k} = w_{k+j-s}$, with seasonality of one week ($s = 7 \cdot 48$), and one day ($s = 48$) were used as reference. The seasonal naïve forecast with $s = 7 \cdot 48$ leads to a mean $\mathrm{PRMSE}_{24} = 0.050\,\mathrm{pu}$, (standard deviation: 0.019 pu) which is better than the seasonal naïve forecast with $s = 48$. The best results could be achieved with the SARIMA model, where the mean $\mathrm{PRMSE}_{24} = 0.041\,\mathrm{pu}$ is about 23 % less and standard deviation 0.015 pu about 25 % lower than with the seasonal naïve method for $s = 7 \cdot 48$. Thus, the increased computational effort of the SARIMA model pays off.

The fact, that the residuals of both forecasts did not pass the Kolmogorov–Smirnov test for normality (see Fig. 3) motivated us to use a scenario-based approach. In this approach, the forecast distribution is derived through MC simulations with random residuals from the model fit.

III. Scenario Reduction

Branches of forecast scenarios (scenario fans) were created in Section II. To obtain a good representation of the probability distribution, a big number of scenarios is desirable. In contrast, for the MPC in Section IV a small number of scenarios is wanted, to keep the computing effort manageable. To comply with both needs, a scenario fan with a high number of MC forecasts is generated and then reduced to a *scenario tree* wherein scenarios are not equiprobable.

A way to create scenario trees is the forward selection algorithm introduced in [12]. Roughly speaking, neighbouring scenarios are clustered together to form a tree-like structure, known as a scenario tree, which naturally imposes time-causality to this representation of uncertainty. The algorithm offers a computationally tractable way to obtain a scenario

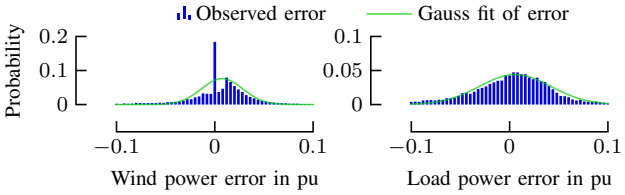

Fig. 3. Error distribution of *all* $\mathrm{SARIMA}(\chi_p, d, \chi_q, s, \chi_P, \chi_Q)$ load and $\mathrm{ARIMA}(\chi_p, 0, \chi_q)$ wind power forecasts. The peak at 0 pu in wind power is due to the saturation for wind speed lower 2.5 m/s and higher 12 m/s.

tree whose distance (in the Wasserstein-Kantorovitch sense) from the original probability distribution, described by the fan, is approximately minimized [12]. In Fig. 2 the scenario fans with the corresponding trees are shown on the right.

The node of a probability tree at time $k|k$ is called *root* and those at stage $k+J|k$ the *leaves*. Scenarios are sequences of admissible wind power and load values spanning from the root node to the leaves. The number of nodes at $k+j|k$ is denoted by $\nu(k+j|k)$ for all $j = 0, \ldots, J$ and the set of all nodes by $\mathbb{S}$. Non-leaf nodes have a set of *children*; we denote the set of child nodes of the l-th node at stage $k+j|k$ by $\mathrm{ch}(l, k+j|k) \subseteq \mathbb{N}_{[1,\nu(k+j+1|k)]}$. The probability to visit node l at $k+j|k$ starting from the root node is $p^{(l)}_{k+j|k}$. Clearly, $\sum_{l=1}^{\nu(k+j|k)} p^{(l)}_{k+j|k} = 1$, and $\sum_{m\in\mathrm{ch}(l,k+j|k)} p^{(m)}_{k+j+1|k} = p^{(l)}_{k+j|k}$. The control actions $\delta^{(l)}_{k+j|k}$ and $u^{(l)}_{k+j|k}$ at $k+j|k$ for node l are causal control strategies and depend on the systems state at $k+j|k$ and the scenario tree running through that node.

Naturally, forecasts in the near future are more accurate than long term predictions. Therefore, using a tree with less nodes in the beginning is advantageous. To obtain this behaviour the branching factor $b = (b_1, b_2, \ldots, b_J)$, that determines the maximum number of children per stage, can be used. Note that due to the non-linear relation in wind speed and power, the scenario tree is generated at every time the optimization problem is solved.

IV. Stochastic MPC

In this section, a SMPC approach is presented to find the optimal control inputs for islanded MGs w.r.t. the scenario trees obtained beforehand. We start with some assumptions.

A. Assumptions

Subsequently, we assume that *a*) DC power flow can be used; the storage units' self discharge and conversion losses are negligible and that the error introduced by this simplification is small compared to the uncertainty that comes from the load and the RES; *b*) thermal and storage units can form the grid and run as parallel voltage sources, providing voltage and frequency; if they run in parallel, they share the deviations (driving them away from their power setpoint) that are caused by load and RES, in a decentralized manner, e.g., through droop control as in [16]; this power sharing is assumed to be instantaneous; *c*) the non-negligible time constants of the storage dynamics that describe the charging and discharging are in the range of several minutes;

TABLE I

EFFECTIVE DISTURBANCE FOR DIFFERENT SETPOINTS

Case	*a*)	*b*)	*c*)
$\bar{w}^{(1)}_{i,k+j\|k}$	0	$\tilde{w}^{(1)}_{i,k+j\|k} - u^{(1)}_{i,k+j\|k}$	$\tilde{w}^{(1)}_{i,k+j\|k} - u^{(1)}_{i,k+j\|k}$
$\bar{w}^{(2)}_{i,k+j\|k}$	0	0	$\tilde{w}^{(2)}_{i,k+j\|k} - u^{(1)}_{i,k+j\|k}$

thus, repeating the control action at the same time scale is sufficient.

B. Microgrid model

We use the MG model introduced by [9]. Hence, we work in a discrete-time framework with a sampling interval t_s. The observable state vector x_k represents the energy that the storage units contain at time kt_s. The real valued input $u_k = (u_{T,k}^T, u_{S,k}^T, u_{R,k}^T)^T \in \mathbb{R}^v$ with $u_{T,k} \in \mathbb{R}^t$, $u_{S,k} \in \mathbb{R}^s$ and $u_{R,k} \in \mathbb{R}^r$ depict the power set points for the thermal, storage and RES units, respectively with $v = t + s + r$. Similarly, the Boolean input $\delta_k = (\delta_{T,k}^T, \delta_{S,k}^T, \delta_{R,k}^T)^T \in \mathbb{B}^v$ with $\delta_{T,k} \in \mathbb{B}^t$, $\delta_{S,k} \in \mathbb{B}^s$ and $\delta_{R,k} \in \mathbb{B}^r$ indicates which thermal, storage and RES units are connected to the islanded MG. The input variables share the dependency $\delta_{i,k} = 0 \Rightarrow u_{i,k} = 0$ for $i \in \mathbb{N}_{[1,t+s+r]}$. The disturbances are $w_k = (w_{D,k}^T, w_{R,k}^T)^T$, where $w_{D,k} \in \mathbb{R}^d$ denotes the error introduced by the load and $w_{R,k} \in \mathbb{R}^r$ the disturbances coming from the RES.

C. Disturbance modelling

The disturbances from load and RES are of different nature. The predicted infeed $\bar{u}^{(m)}_{i,k+j|k}$ of RES unit i is limited by the set point $u^{(l)}_{i,k+j|k}$ for $m \in \mathrm{ch}(l, k+j|k)$. In this case, the predicted *effective disturbance* $\bar{w}^{(m)}_{i,k+j|k}$ is the difference between the limit $u^{(l)}_{i,k+j|k}$ and the predicted infeed $\bar{u}^{(m)}_{i,k+j|k}$. Naturally, if the predicted RES power $\tilde{w}^{(m)}_{i,k+j|k}$ is above the limit $u^{(l)}_{i,k+j|k}$, the effective disturbance is zero as the power infeed equals the limitation. This can be described by

$$\bar{w}^{(l)}_{i,k+j|k} = \min(0, \tilde{w}^{(m)}_{i,k+j|k} - u^{(l)}_{i,k+j|k}). \tag{2a}$$

If there are, for instance, two disturbances $\tilde{w}^{(1)}_{i,k+j|k}$, $\tilde{w}^{(2)}_{i,k+j|k}$ and the predicted setpoint of the machines is $u^{(1)}_{i,k+j|k}$ then the effective disturbances $\bar{w}^{(1)}_{i,k+j|k}, \bar{w}^{(2)}_{i,k+j|k}$ change as indicated by Table I: *a*) if the power limit of the RES unit $u^{(1)}_{i,k+j|k}$ is below both $\tilde{w}^{(1)}_{i,k+j|k}$ and $\tilde{w}^{(2)}_{i,k+j|k}$, then the predicted effective disturbances are zero as the infeed in both scenarios can be guaranteed and equals $u^{(1)}_{i,k+j|k}$; *b*) if $u^{(1)}_{i,k+j|k}$ is between the two scenarios, the effective disturbance is $\bar{w}^{(1)}_{i,k+j|k} \leq 0$, as the unit's predicted infeed is below $u^{(1)}_{i,k+j|k}$ and as $\tilde{w}^{(2)}_{i,k+j|k}$ is above $u^{(1)}_{i,k+j|k}$, $\bar{w}^{(2)}_{i,k+j|k}$ is zero; and *c*) if both $\tilde{w}^{(1)}_{i,k+j|k}$ and $\tilde{w}^{(2)}_{i,k+j|k}$ are below $u^{(1)}_{i,k+j|k}$, both predicted effective disturbances equal the difference between setpoint and forecast.

In contrast, the predicted load power cannot be influenced by any input. Therefore,

$$\bar{w}^{(l)}_{D,k+j|k} = \tilde{w}^{(l)}_{D,k+j|k}. \tag{2b}$$

D. Power and power sharing

In islanded mode, to ensure the local power balance, the grid-forming units adapt their power output $\bar{u}^{(m)}_{k+j|k}$ with respect to the disturbances $\bar{w}^{(m)}_{k+j|k}$. Therefore, the predicted power of the units is composed of the setpoint $u^{(l)}_{k+j|k}$ and a share of the disturbances ($\mathbf{H}^{(l)}_{k+j|k}\bar{w}^{(m)}_{k+j|k}$) as follows.

$$\bar{u}^{(m)}_{k+j|k} = u^{(l)}_{k+j|k} + \mathbf{H}^{(l)}_{k+j|k}\bar{w}^{(m)}_{k+j|k}, \tag{3a}$$

for all $m \in \mathrm{ch}(l, k+j|k)$, $l \in \mathbb{S}$. As disabled units cannot adjust their power, their corresponding rows in $\mathbf{H}^{(l)}_{k+j|k}$ have entries zero. Enabled units adjust their power with respect to a weighting vector $u_{\mathbf{H}} \in \mathbb{R}^v_{0+}$ that is chosen, for instance, corresponding to the units' nominal power. With $\mathbf{U_H} = \mathrm{diag}\,(u_{\mathbf{H}})$ this behaviour can be modelled by choosing $\mathbf{H}^{(l)}_{k+j|k}$ in (3a) to be the following.

$$\mathbf{H}^{(l)}_{k+j|k} = -\frac{\mathbf{U_H}\delta^{(l)}_{k+j|k}}{u_{\mathbf{H}}^T\delta^{(l)}_{k+j|k}}\mathbf{1}^T_{(d+r)1} + \mathrm{diag}\left(\mathbf{0}_{(t+s)d}, \mathbf{I}_r\right), \tag{3b}$$

where the first summand represents the power sharing of grid-forming units and the second the change of RES power [10]. The effective power of the units $\bar{u}^{(m)}_{k+j|k}$, is bounded by $u^{\min}, u^{\max} \in \mathbb{R}^v$ if the corresponding unit is enabled, i.e., for all $m \in \mathrm{ch}(l, k+j|k)$,

$$\mathrm{diag}\left(u^{\min}\right)\delta^{(l)}_{k+j|k} \leq \bar{u}^{(m)}_{k+j|k} \leq \mathrm{diag}\left(u^{\max}\right)\delta^{(l)}_{k+j|k}. \tag{3c}$$

E. System dynamics

The system dynamics is given by

$$x^{(m)}_{k+j+1|k} = \mathbf{A}x^{(l)}_{k+j|k} + \mathbf{B}\bar{u}^{(m)}_{k+j|k}, \tag{4a}$$

for all $m \in \mathrm{ch}(l, k+j|k)$, and $x^{(1)}_{k|k} = x_k$. To model the dynamics of the storage units, we choose $\mathbf{A} = \mathbf{I}_s$ and $\mathbf{B} = -t_s(\mathbf{0}_{st}, \mathbf{I}_s, \mathbf{0}_{sr})$. The states are bounded by $x^{\min}, x^{\max} \in \mathbb{R}^s$ that result from the limited storage capacity. Hence,

$$x^{\min} \leq x^{(m)}_{k+j+1|k} \leq x^{\max}. \tag{4b}$$

To ensure feasibility of the problem (4b) is imposed as a soft constraint.

F. DC power flow

DC power flow (see [10], [17]) is used to link the power at the bus bars $\bar{u}^{(m)}_{k+j|k}$ and $\bar{w}^{(m)}_{D,k+j|k}$ with the power flow over the lines $o^{(m)}_{k+j|k}$, given by

$$o^{(m)}_{k+j|k} = \mathbf{F} \cdot ((\bar{u}^{(m)}_{k+j|k})^T, (\bar{w}^{(m)}_{D,k+j|k})^T, \mathbf{0}^T_{n1})^T, \tag{5a}$$

with $\mathbf{F} \in \mathbb{R}^{e\times(h+d+n)}$, where e is the number of edges in the grid, and n the number of passive network nodes. The power flow is limited by $o^{\min} \in \mathbb{R}^e$ and $o^{\max} \in \mathbb{R}^e$, i.e.,

$$o^{\min} \leq o^{(m)}_{k+j|k} \leq o^{\max}. \tag{5b}$$

To ensure a local power balance, additionally

$$0 = \mathbf{1}^T_{v1} \cdot ((\bar{u}^{(m)}_{k+j|k})^T, (\bar{w}^{(m)}_{D,k+j|k})^T, \mathbf{0}^T_{n1})^T \tag{5c}$$

must hold.

G. Optimal control problem

The generator costs were modelled according to [18]. The cost function for $m, l \in \mathbb{M}$, where $\mathbb{M} \subset \mathbb{S}$ is the set of all

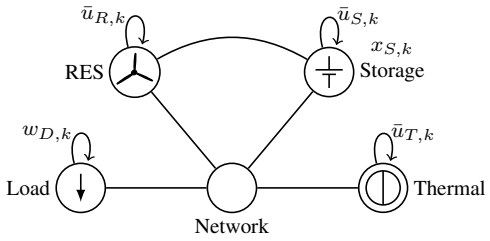

Fig. 4. Microgrid considered for case study.

nodes of the tree except the root, and $a \in \mathbb{S}$ is given by

$$J^{(m)}_{k+j|k} = p^{(m)}_{k+j|k}(c_0^T \delta^{(l)}_{k+j|k} + c_1^T \bar{u}^{(m)}_{k+j|k} + (\bar{u}^{(m)}_{k+j|k} - u^d)^T \operatorname{diag}(c_2)(\bar{u}^{(m)}_{k+j|k} - u^d) + (\delta^{(l)}_{k+j|k} - \delta^{(a)}_{k+j-1|k})^T \operatorname{diag}(c_{sw})(\delta^{(l)}_{k+j|k} - \delta^{(a)}_{k+j-1|k})), \quad (6)$$

where $m \in \mathrm{ch}(l, k+j|k)$ and $l \in \mathrm{ch}(a, k+j-1|k)$. Further, $p^{(m)}_{k+j|k} \in \mathbb{R}$ is the probability of disturbance $\tilde{w}^{(m)}_{k+j|k}$, $c_0, c_1, c_2 \in \mathbb{R}^v$ are weights and $u^d \in \mathbb{R}^v$ is a vector with $u^d = (\mathbf{0}^T_{(t+s)1}, (u^d_R)^T)^T$, where u^d_R is the desired RES infeed, i.e., in normal operation the nominal value of the unit. The last line of (6) represents the costs for switching a machine on or off with $c_{sw} \in \mathbb{R}^v$.

The overall costs are the weighted sum over all stages, for all $m \in \mathbb{M}$ with a weighting factor $\gamma \in (0,1) \subset \mathbb{R}$ to emphasize near decisions over those in the far future. A MPC strategy is used to find the optimal inputs at instant k and apply the resulting $(u_k, \delta_k) = (u^{(1)}_{k|k}, \delta^{(1)}_{k|k}) = f(\tilde{w}, \tilde{p}, x_k, \delta_{k-1})$ to the system. Naturally, this leads to a receding horizon control strategy. With $J^{(m)}_{k+j|k}$ from (6) and the $\mathrm{stage}(m)$ function that indicates the optimization time instant j of node m the corresponding optimal control problem reads as follows.

Problem 1 (Scenario-based SMPC): Find the optimal inputs $(u^{(m)}_{k+j|k}, \delta^{(m)}_{k+j|k})^*$ for $j \in \mathbb{N}_{[1,J]}$ that minimize

$$J_c = \sum_{m \in \mathbb{M}} \gamma^j J^{(m)}_{k+j|k} \text{ with } j = \mathrm{stage}(m) \text{ and} \quad (7)$$

subject to the constraints (2)–(5).

V. Case Study

To assess the performance, the proposed SMPC will be compared to the minimax MPC (MMPC) presented in [10] and a control policy based on a hypothetical perfect forecast that is used as a reference. A certainty-equivalence approach where the mean value of a non-perfect forecast is employed was not considered as it led to significant violations of constraints in the operation in [9]. Subsequently, all values are normalized to a power of 1 pu and a time of 1 h.

The MG used (see Fig. 4) comprises a load with $w_{D,k}$, a thermal generator with power $\bar{u}_{T,k}$, a RES with $\bar{u}_{R,k}$ and a storage unit with $\bar{u}_{S,k}$ and stored energy $x_{S,k}$. Hence, $\bar{u}_k = (\bar{u}_{T,k}, \bar{u}_{S,k}, \bar{u}_{R,k})^T$, $w_k = (w_{D,k}, w_{R,k})^T$ and $x_k = x_{S,k}$. The limits are $u^{\min} = (0.4, -1, 0)^T$, $u^{\max} = (1, 1, 2)^T$, $x^{\min} = 0$ and $x^{\max} = 6$ as well as $o_i^{\max} = -o_i^{\min} = 1.3$ for $i = 1, \ldots, 5$. A sampling time of $t_S = 30\,\mathrm{min}$ was chosen, leading to $\mathbf{B} = (0, -0.5, 0)$. Further, $\mathbf{A} = 1$ and $u_{\mathbf{H}} = (1, 1, 0)^T$. The initial conditions $\delta_{-1} = (0, 1, 1)^T$ and

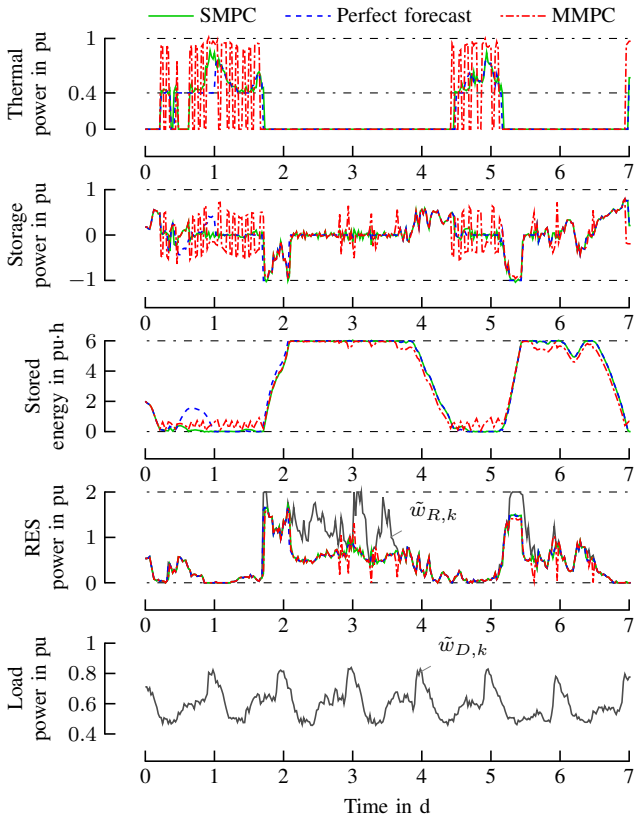

Fig. 5. Thermal, storage, renewable and load power as well as stored energy with different MPC approaches.

$x_0 = 2$ were assumed. To cover a full charge or discharge of the storage unit, $J = 12$ for all MPC schemes. For the objective function, the generator running costs from [18] were normed to the size of the unit, i.e., $c_0 = (0.1178, 0, 0)^T$, $c_1 = (0.7510, 0, 0)$ and $c_2 = (0.0048, 0, 0.2)$. Further, $u^d = (0, 0, 2)$, $\gamma = 0.95$ and $c_{\mathrm{sw}} = 0.3$ were chosen.

To speed up the computation, the binary variables of the SMPC were fixed for optimization time instants $j > 3$. For $j \leq 3$, binaries exist. For all $j > 3$ all entries of δ are fixed to one, and the minimum power of the thermal units is set to zero. Further, a branching factor of $b = (8, 2, 2, 1, \ldots, 1)$ was employed. As extensive simulation studies showed that storage and RES units are always turned on, their switching variables were fixed to $\delta_{S,k} = 1$ and $\delta_{R,k} = 1$ for all $k \in \mathbb{N}_0$. Consequently, only the thermal unit is switched on and off.

The number of MC forecast scenarios was set to 500 and the robust interval of the MMPC was chosen such that it contains 99 % of the forecast scenarios. A sensitivity study, using the 95 % confidence interval for the MMPC showed only a slight decrease of 0.1 % in terms of costs, compared to the 99 % interval and more constraint violations with the smaller interval. Hence, the choice is reasonable.

The scheme in Fig. 1 was implemented in MATLAB® using the econometrics toolbox, Yalmip [19], and Gurobi as a numerical solver. The maximum runtime for one execution, including forecast, scenario reduction and optimization was less than 2 min for all steps with an Intel® Core™ i5-3320M processor @ 2.6 GHz and 8 GB RAM. As this time is

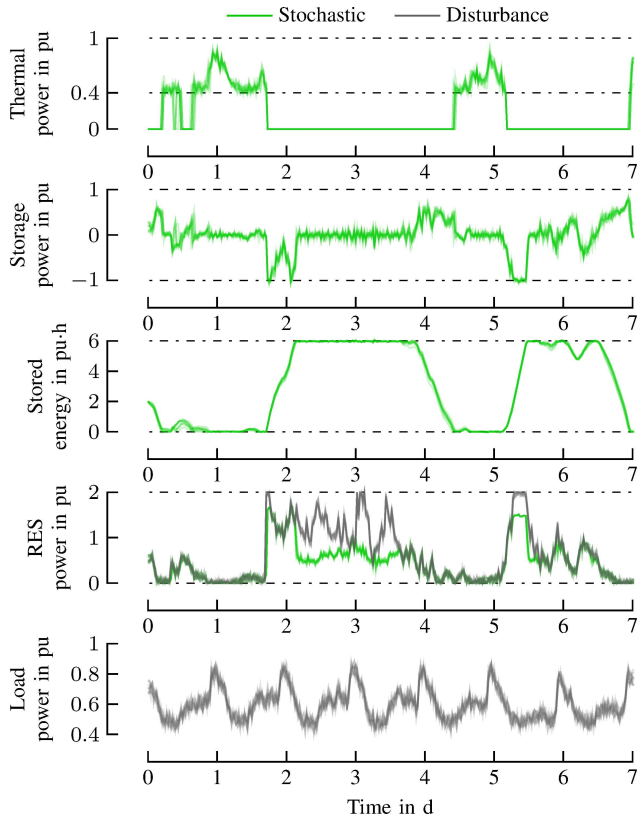

Fig. 6. Sensitivity analysis of SMPC, where load and RES of the model were altered for every time step with a random, normally distributed disturbance of ±5 % of their nominal value.

significantly smaller than the sampling interval of 30 min, the optimization is adequately fast and hence applicable.

The sensitivity analysis in Fig. 6 showed that the SMPC approach may lead to small constraint violations of less than 3 % of the nominal value. For the case study in Fig. 5, a total of 19 violations occurred during one week because the SMPC approach can only assure that the probability of violations is small. The occurrence could be minimized by using a more complex scenario tree or tighten the constraints. For now, as the violations are very small, it is assumed that they lie in the power and energy tolerances that the units can handle.

Comparing the MMPC from [10] with the SMPC over 7 days in Table II, the renewable infeed could be increased by 2 %. Further, thermal energy could be decreased by 13 % and the gap to the reference with perfect forecast knowledge could be reduced significantly. Additionally, the number of switching actions was decreased, which leads to a decrease of maintenance costs. This also shows in the reduction of the accumulated operation costs of 7 % that were calculated with (6) and the MG's simulated power values.

VI. Conclusions

This paper studied the scenario-based model predictive operation control of islanded MGs. A new stochastic approach, composed of a forecast, a scenario reduction and stochastic optimization was presented. The provided numerical case study indicates that the new approach leads to a significant decrease of running costs. Future work will address the prediction of solar power. Also, a combination of a worst case and a stochastic approach to ensure safe operation will be considered. Additionally, the scalability of the approach will be investigated to see if it can be used to operate MGs with more nodes.

TABLE II

Overall renewable and thermal infeed of simulation

	Perfect forecast	SMPC	MMPC
Operation costs	158.7	160.5	172.1
Renewable energy in pu h	150.6	149.2	146.7
Thermal energy in pu h	53.1	54.6	62.7
Thermal switching	5	9	39

References

[1] REN21 Secretariat, "Renewables 2014 global status report," REN21, Paris, Tech. Rep., 2014.

[2] R. H. Lasseter, "MicroGrids," in *IEEE PES Winter Meeting*, vol. 1, 2002, pp. 305–308.

[3] J. A. Peças Lopes, C. L. Moreira, and A. G. Madureira, "Defining control strategies for microgrids islanded operation," *IEEE Trans. Power Syst.*, vol. 21, no. 2, pp. 916–924, 2006.

[4] I. Moghram and S. Rahman, "Analysis and evaluation of five short-term load forecasting techniques," *IEEE Trans. Power Syst.*, vol. 4, no. 4, pp. 1484–1491, 1989.

[5] S. Rahman and R. Bhatnagar, "An expert system based algorithm for short term load forecast," *IEEE Trans. Power Syst.*, vol. 3, no. 2, pp. 392–399, 1988.

[6] J. Palomares-Salas, J. De la Rosa, J. Ramiro, J. Melgar, A. Aguera, and A. Moreno, "Arima vs. neural networks for wind speed forecasting," in *IEEE CIMSA'09*, 2009, pp. 129–133.

[7] A. Parisio and L. Glielmo, "Stochastic model predictive control for economic/environmental operation management of microgrids," in *ECC*, 2013, pp. 2014–2019.

[8] S. Mohammadi, S. Soleymani, and B. Mozafari, "Scenario-based stochastic operation management of microgrid including wind, photovoltaic, micro-turbine, fuel cell and energy storage devices," *Int. J. Electr. Power Energy Syst.*, vol. 54, pp. 525–535, 2014.

[9] C. A. Hans, V. Nenchev, J. Raisch, and C. Reincke-Collon, "Minimax model predictive operation control of microgrids," in *19th IFAC WC*, Cape Town, South Africa, 2014, pp. 10 287–10 292.

[10] ——, "Approximate closed-loop minimax model predictive operation control of microgrids," in *ECC*, Linz, Austria, 2015, pp. 241–246.

[11] G. E. Box, G. M. Jenkins, and G. C. Reinsel, *Time series analysis: forecasting and control*. John Wiley & Sons, 2013.

[12] H. Heitsch and W. Römisch, "Scenario reduction algorithms in stochastic programming," *Comput. Optimization. Appl.*, vol. 24, no. 2-3, pp. 187–206, 2003.

[13] D. Bernardini and A. Bemporad, "Scenario-based model predictive control of stochastic constrained linear systems," in *48th IEEE CDC & 28th CCC*, 2009, pp. 6333–6338.

[14] Atmospheric Radiation Measurement (ARM) Climate Research Facility. Surface Meteorology System (MET). June 2009–Oct. 2009, 39° 5' 28" N, 28° 1' 45" W: Eastern North Atlantic Facility, windspeed. ARM Data Archive: Oak Ridge, Tennessee, USA. Data set accessed 2011-07-14 at `www.arm.gov`.

[15] M. Kazemi and A. Goudarzi, "A novel method for estimating wind turbines power output based on least square approximation," *Int. J. Eng. Adv. Technol.*, vol. 2, no. 1, pp. 97–101, oct 2012.

[16] J. Schiffer, R. Ortega, C. A. Hans, and J. Raisch, "Droop-controlled inverter-based microgrids are robust to clock drifts," in *ACC*, Chicago, IL, USA, 2015, pp. 2341–2346.

[17] K. Purchala, L. Meeus, D. Van Dommelen, and R. Belmans, "Usefulness of dc power flow for active power flow analysis," in *IEEE PES GM*. IEEE, 2005, pp. 454–459.

[18] M. Živić Đurović, A. Milačić, and M. Kršulja, "A simplified model of quadratic cost function for thermal generators," *Ann. DAAAM 2012 Proc. 23rd Int. DAAAM Symp.*, vol. 23, no. 1, pp. 25–28, 2012.

[19] J. Löfberg, "Yalmip: A toolbox for modeling and optimization in matlab," in *2004 IEEE CACSD*. IEEE, 2004, pp. 284–289.